Exploiting the continuity equation for mechanistic understanding through spatially resolved SSITKA-DRIFTS

The role of carbonyls in RWGS over Pt/CeO_2

Vico van Berkel, Damián; Urakawa, Atsushi

DOI
10.1016/j.jcat.2024.115470

Publication date
2024

Document Version
Final published version

Published in
Journal of Catalysis

Journal of Catalysis 433 (2024) 115470

Contents lists available at ScienceDirect

Journal of Catalysis

journal homepage: www.elsevier.com/locate/jcat

Research article

Exploiting the continuity equation for mechanistic understanding through spatially resolved SSITKA-DRIFTS: The role of carbonyls in RWGS over Pt/CeO_2

Damián Vico van Berkel, Atsushi Urakawa *

Catalysis Engineering, Department of Chemical Engineering, Delft University of Technology, Van der Maasweg 9, 2629 HZ Delft, the Netherlands

A B S T R A C T

Insight into mechanisms of heterogeneously catalyzed reactions holds importance in the development and optimization of new catalytic materials. Yet, the approaches often used in such investigations heavily rely on assumptions concerning the reactor and kinetics. Herein we report a new kind of kinetic investigation taking CO_2 hydrogenation reaction, specifically the reverse water–gas shift (RWGS) reaction over 3 wt% Pt/CeO_2, as an exemplifying case. The reported approach is based on spatially resolved steady-state isotopic transient kinetic analysis (SSITKA) and diffuse reflectance infrared Fourier transform spectroscopy (DRIFTS) identifying gaseous/surface species and their spatial variations along the reactor. This approach allows accurate evaluation of reaction mechanism by identifying correlations among the concentrations of gaseous/surface species and by quantitative description of their spatial variations by a kinetic model. Spatially resolved SSITKA-DRIFTS experiments show carbonate decomposition via a Pt-bound carbonyl to be the main route towards the production of carbon monoxide. Further kinetic modeling of the spatially resolved data confirms this mechanism proposal, and points to the production of water as the rate-limiting step.

1. Introduction

The significant weight of catalysis in economy and sustainability within the chemical industry has motivated the adaptation and upgrading of catalyst design, in which rationale is applied rather than brute force. Such fundamental goal is, however, hampered by the intrinsic complexity involved in understanding the behavior of a heterogeneous catalyst, arising from the vast network of phenomena and parameters influencing catalytic activity (e.g. reaction rate and network, mass and heat transport, concentration and temperature gradient on both the pellet and reactor scales, material's geometrical and electronic structures, operating conditions including reactor type) [1]. These mutually influencing factors contribute to the difficulty in determining intrinsic reaction mechanisms and kinetics. For example, the elucidation of different elementary steps involved in surface-catalyzed reactions can be obfuscated by the influence of transport phenomena such as mass transfer limitations [2,3]. For mechanistic studies, with the aim to discern catalytically active species and dormant (i.e. spectator) ones, the application of transient techniques coupled with *operando* spectroscopy methodologies by means of modulation-excitation technique and isotope labeling has gained popularity [4–6]. For the determination of intrinsic kinetic parameters as well as plausible reaction mechanisms, steady-state isotopic transient kinetic analysis (SSITKA), involving switch in the concentration of isotopomers, constitutes an attractive technique, as the reaction environment is not perturbated from the chemical potential point of view (thus steady-state, neglecting kinetic isotope effects) [7–10]. This is of crucial importance, as the role of different surface species might depend on the composition of the reaction atmosphere, as shown by Meunier et al. who demonstrated that the reactivity of carbonates on ceria depends on the nature of the feed [11]. In addition, SSITKA coupling with *operando* vibrational spectroscopy readily expands the more precise mechanistic insight by providing key information on the nature of active species, typically investigated by IR [12–14]. However, an important factor generally overlooked in the state-of-the-art kinetic studies is that packed-bed reactors, the most common reactor configuration in heterogeneous catalysis and SSITKA studies, are governed by the continuity equation, which directly stipulates the presence of gradients within the catalytic reactor. In other words, solely probing one point in the reactor does not guarantee a complete picture of the reaction mechanism at hand, as mechanistic, redox state, temperature gradients could be present [15–18]. The same holds for the kinetic study despite the use of low conversion (i.e. differential) conditions, which constitutes the go-to approach for kinetic studies. Even though their application can yield important insights into reaction mechanisms, carrying out kinetic studies under industrially attractive conversions can yield important insight into the reactor-

* Corresponding author.
E-mail address: A.Urakawa@tudelft.nl (A. Urakawa).

https://doi.org/10.1016/j.jcat.2024.115470
Received 30 November 2023; Received in revised form 23 February 2024; Accepted 25 March 2024
Available online 29 March 2024

catalyst relationship, and provide answers to unclear insights gained under the low conversion regime.

In this work, we report the combination of SSITKA with spatiotemporally resolved diffuse reflectance infrared Fourier transform spectroscopy (DRIFTS) and gas sampling as a powerful tool towards the elucidation of the reaction mechanisms and kinetics. With the reverse water–gas shift (RWGS) reaction over Pt/CeO_2 as a probe reaction, we show the importance of considering the chemistry throughout the entire catalyst bed, providing key insight into the role of different intermediates and a more complete extraction of the kinetic parameters. The latter is aided by kinetic simulations, in which the required optimization procedures are based on the spatiotemporally resolved data, constituting, to the best of our knowledge, the first model of its kind.

2. Experimental

2.1. Catalyst synthesis

Pt/CeO_2 catalyst was prepared by incipient wetness impregnation. The selected support were impregnated with a 72 mM $[Pt(NH_3)_4](NO_3)_2{\cdot}H_2O$ precursor solution. The resulting solid was dried at 80 °C for 24 h and then calcined at 500 °C for 5 h. The obtained catalyst powder was pelletized at 10 tf cm^{-2}, crushed, and sieved to a particle size range between 212 and 300 μm.

2.2. Catalytic tests

The catalytic tests were performed using a quartz bed reactor of 4 mm internal diameter, placed horizontally within the spatial sampling module. Heating was provided by a BOSCH hot-gas blower with a reflective material to achieve homogeneous heating of the reactor. Step switches to each isotopically labeled reactant feed were introduced through a VICI Valco four-way switching valve controlled through LabVIEW. Flow of all reactants were controlled by EL-FLOW Select Bronkhorst digital mass flow controllers (MFC) (Figure S1).

The catalyst bed was packed between quartz wool at both ends in order to ensure the fixation of the catalyst particles and the pre-heating of the gases. The experiments were preceded by activation of the catalyst by *in situ* reduction at 300 °C under 10 % H_2 in He (50 mL min^{-1}) for one hour after heating the bed at a rate of 10 °C min^{-1} under He flow. Consecutively, the catalyst bed was flushed with 30 mL min^{-1} pure He for removal of weakly bound hydrogen species.

The concentrations of CO_2 and H_2 were 2.25 and 9 vol%, respectively. The selected isotopically labeled reactant was $^{13}CO_2$ (Cambridge Isotope Laboratories, 99.7 %). Helium was used as carrier gas, and an inert tracer of 2.5 vol% Ar was included within the $^{13}CO_2$-containing stream. The total flow rate was 50 mL min^{-1}. Outlet gas concentration profiles were measured by a Bruker ALPHA-II Compact FT-IR spectrometer, equipped with a gas-phase cell. Spectra were acquired at 4 cm^{-1} resolution and 5 s time resolution. The switch to each stream was carried out multiple times, allowing cycle averaging and a subsequent increase in signal-to-noise (S/N) ratio.

2.3. Spatially resolved SSITKA

Isotopically labeled experiments were concurrently evaluated in a spatially resolved fashion through a Pfeiffer Vacuum Omnistar mass spectrometer, attached to a stainless steel capillary (I.D.: 500 μm, O.D.: 700 μm, REACNOSTICS GmbH) inserted inside the catalyst bed. Movement of the gas-sampling capillary was achieved through a set of actuators (ZABER) with 1 μm resolution (P_1 = 0.5 mm, P_2 = 2.5 mm, P_3 = 4.5 mm, P_4 = 6.5 mm). Sampling of selected *m/z* fragments was achieved through the four concentric 50 μm holes within the capillary, which were aligned with the outlet position of the bed prior to any experiment. Cycle slicing and evaluation of the true start time of each experiment was achieved through taking the derivative of the Argon response, allowing the identification of the time point at which the Ar response had a non-zero rate (i.e. is detected by MS). Accurate quantitative evaluation of ^{12}C-based species was not possible due to large *m/z* overlap with their ^{13}C counterparts. Concerning the latter, individual contribution of $^{13}CO_2$ and ^{13}CO species was identified through blank experiments carried out at the start of each day. Spatial profiling of temperature was attained through the thermocouple attached at the opposite end of the capillary, and its tip (temperature measurement point) was aligned with the position of the gas sampling holes.

2.4. Spatially resolved SSITKA-DRIFTS

Operando DRIFTS experiments were carried out using a INVENIO FT-IR Bruker spectrometer equipped with a liquid nitrogen-cooled MCT detector. Spectra were acquired with a time resolution of 1.04 s (5 scans with 40 kHz scanner velocity). A custom-built cell set out to imitate the flow patterns within the packed-bed reactor was used [19], with the catalyst inserted between quartz wool as previously explained. The cell equipped with a ZnSe window was placed within a Harrick praying mantis optical system. Spatial resolution was enabled by mounting the entire cell on motorized stages. Respective background spectrum at each position of the catalyst bed was taken under He flow at the selected operating temperature before the start of the SSITKA experiments. Analogously to the gas-sampling experiments, averaging over reproducible cycles was employed in order to increase S/N ratios. Catalyst amount and activation procedure were identical to those of the catalytic test (*vide supra*). The reactor effluent was analyzed by the aforementioned FT-IR spectrometer.

2.5. Kinetic modeling

Additional insights into the reaction mechanism were investigated through kinetic modeling of the attained SSITKA data, entirely carried out within MATLAB. The governing partial and ordinary differential equations, (shown in Supplementary Information S2) were solved and optimized with respect to the experimental data using the Nelder-Mead algorithm and a root mean square error (RMSE) objective function, providing the set of kinetic parameters best fit to describe the experimental data. Moreover, the kinetic modeling was performed using the reactor effluent concentration profiles and their spatially resolved counterparts, to understand possible variations in accuracy stemming from spatial variations of gaseous and surface species and thus reactivity.

3. Results and discussion

3.1. Catalytic activity and effluent-based SSITKA

Figure S3 shows the catalytic activity results. CO_2 conversion of 14.1 % and 19.6 % were obtained at 200 and 250 °C, respectively. Comparison to the equilibrium conversion ($X_{CO2,200}$ = 15.2 % and $X_{CO2,250}$ = 19.6 %) indicates that both experiments lie close to or at the thermodynamic limitation [20,21]. Selectivity towards CO was always > 99.9 %, with no other products such as CH_4 within our detection limit, demonstrating high activity and selectivity of Pt/CeO_2 in RWGS. During the 10 h long operation, the catalysts only suffered a mild deactivation, possibly entailed by carbon deposition and/or Pt sintering. These deactivation patterns have been also portrayed by previous research on RWGS over ceria-supported Pt catalysts [13,22,23].

The nature of the experimental setup allowed the SSITKA experiments to be evaluated through the lens under which traditional reactor-effluent SSITKA studies are carried out, due to the outlet being analyzed with gas-phase IR spectroscopy. Comparison between the ^{12}C- and ^{13}C-based species measured at 200 °C (Fig. 1a) confirmed the maintenance of the overall steady-state once the isotopically labeled stream was inserted into the reactor, as the crossover point occurred at half the

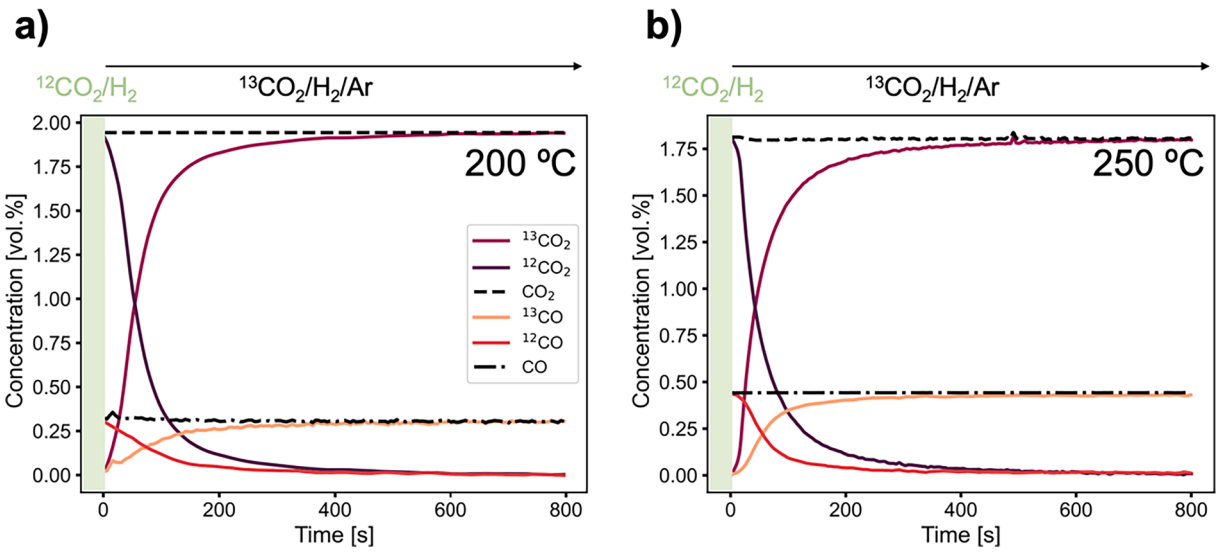

Fig. 1. Outlet concentration profile of carbon-containing species after the switch from $^{12}CO_2/H_2$ to $^{13}CO_2/H_2/Ar$ at a) 200 °C and b) 250 °C. Conditions: $H_2/^xCO_2 = 4$ ($c_{xCO2} = 2.25$ vol%), $c_{Ar} = 2.5$ vol%, $c_{H2} = 9$ vol%, P = 1 bar, $W_{cat} = 180$ mg, F = 50 NmL/min.

steady-state concentration value. Moreover, such behavior also indicates the absence of noticeable kinetic isotope effects (KIE) brought upon the heavier ^{13}C-based species, implying that the rate-determining step (RDS) of the reaction did not involve a carbon-containing bond formation/cleavage [7,24,25]. However, insight into KIE involving ^{13}C-based species is limited due to its complex detection, which may also explain these observations. These results further make apparent a delay of ^xCO profile compared to that of $^xCO_2$ (x = 12 or 13), pointing to the reaction proceeding upon the adsorption of CO_2 and subsequent surface reactions. The slower exchange of CO species can also be correlated to the surface intermediates leading to CO not being directly involved in the RDS.

At higher temperature Fig. 1b, the exchange between isotopically labeled species was faster, directly indicating larger reaction rates at the higher temperature.

3.2. Spatially resolved SSITKA

In order to envisage possible concentration gradients within the reactor, we applied spatially-resolved MS gas sampling to the SSITKA experiments. The CO concentration profiles at the four axial positions are presented in Fig. 2a. Evidently, CO concentration increased at more down-stream bed positions, as its production spans the entire catalyst bed. In other words, the increasing area difference between the responses of CO and Ar with increasing position along the bed directly shows its proportionality to the amount of active surface species, and demonstrates that this reaction path proceeds via surface reactions originating from a surface-bound CO_2 precursor. At the first two positions screened, the productivity of CO was found to be more prominent, leading to 66 % of the overall CO production. Due to the RWGS reaction being endothermic, the possible decrease in temperature at more downstream positions could have explained such variations. However, the spatial temperature profiling (Figure S4) did not support this reasoning as no substantial temperature gradients were present. Therefore, the gradients stem from variations in reaction rate within the bed. This is due to the frontal positions having the largest reactant concentration, promoting their conversion towards CO and H_2O, which subsequently leads to lower reaction rates downstream. In addition, CO is known for readily adsorbing on Pt, which could lead to poisoning of downstream active sites and/or its adsorption on non-catalytically active moieties.

The normalized responses for the product CO, generally used to

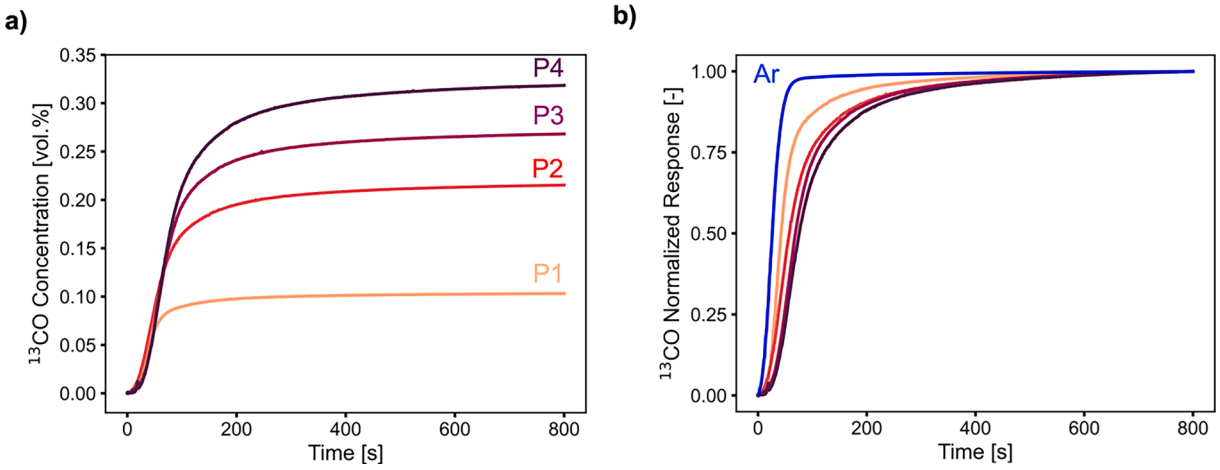

Fig. 2. Spatially resolved gas sampling results attained after a switch from $^{12}CO_2/H_2$ to $^{13}CO_2/H_2/Ar$ at 200 °C over 3 wt% Pt/CeO_2. a) ^{13}CO concentration profiles and b) normalized responses of ^{13}CO. Conditions: $H_2/^xCO_2 = 4$ ($c_{xCO2} = 2.25$ vol%), P = 1 bar, $W_{cat} = 180$ mg, F = 50 NmL/min. $P_1 = 0.5$ mm, $P_2 = 2.5$ mm, $P_3 = 4.5$ mm, $P_4 = 6.5$ mm.

evaluate the kinetics within SSITKA studies as they serve as a direct measure of the exchange rates [4,26,27], attained upon a switch from $^{12}CO_2/H_2$/He to $^{13}CO_2/H_2$/Ar/He at 200 °C are shown in Fig. 2b. An observable delay between $^{13}CO_2$ and Ar suggests the strong reversible interaction of CO_2 with the catalyst [20,23]. Concerning spatial variations, the surface lifetime or mean surface residence time ($\tau_{0.5}$), near the front of the bed was roughly 35 s shorter than that near the outlet, indicating the presence of noticeable variations in reaction rate throughout the catalyst bed. These differences may be attributed to the presence of larger concentrations of the reactants towards the inlet position. However, merely investigating gaseous species provides no insight into possible surface intermediates, indicating the need for multimodal approaches [28].

3.3. Surface species quantification

SSITKA readily allows the quantification of surface intermediates (N_{COx}) leading to a specific product [4]. Traditionally, the area between the inert tracer and the response of the reactant and product are assumed directly proportional to the amount of surface intermediates that lead to CO(g) [29–31]. However, if only reactor effluent SSITKA is conducted, a sole value for the coverage of such species is obtained. As depicted by the continuity equation, this is inherently not accurate, and only serves as a cumulative value throughout the entire catalyst bed, lacking any insight into how this value proceeds throughout the bed. Therefore, we computed these values throughout the entire bed on a per-position basis, for which the results are shown in Fig. 3, using the methodology described in Supplementary Information S4.2. The conversion from surface concentration to coverage was carried out through employing the dispersion values attained through CO chemisorption measurements (63 %).

Fig. 3 shows that the coverage of both CO_2 and CO surface species is largest at the inlet position, in line with the expectations of larger reaction rates at these positions. Interestingly, for CO_2 the coverage on Pt is always larger than unity, which can be translated to the amount of Pt sites simply not being enough to account for all the adsorbed CO_2 species [20,32]. In other words, another site is responsible for the adsorption of CO_2, suggesting that it occurs on the support rather than on the metal, as previously established in RWGS studies over reducible support-based catalysts of metals with low oxophilicity such as Pt [20,30,33]. The large CO_2 coverages obtained could also indicate the inability for all surface CO_2 species to undergo reaction, suggesting that a pool of adsorbed CO_2 might lie in sites away from Pt and therefore can not undergo hydrogenation. Concerning adsorbed CO species, the amount of Pt sites is enough to explain all of the CO(g) formed, pointing to a direct role of Pt. Therefore, the involvement of Pt and the apparent activation of CO_2 by the support indicates the importance of the platinum-ceria interface and/or the support sites vicinal to the metal nanoparticles [34].

3.4. Spatially resolved SSITKA-DRIFTS

Surface intermediates formed during the RWGS over Pt/CeO_2 were studied by *operando* DRIFTS concurrently to the isotopic switches, allowing to relate the formation of CO to the responses of surface species. SSITKA-DRIFTS readily allows to discern active species from dormant (and less active) species, as only those that undergo a reaction (not necessarily towards the product) will potentially showcase an exchange towards their isotopically labeled counterpart, while spectators species remain undisturbed at the surface [27].

The DRIFT spectra under both $^xCO_2 + H_2$ feeds over Pt/CeO_2 at 200 °C are presented in Fig. 4. Within the ν(CO) region (Fig. 4a), a band at 2005 cm^{-1} was observed under the $^{12}CO_2$-containing feed, ascribed to linear carbonyls on Pt [35–38]. However, these bands are noticeably red-shifted with respect to usual carbonyl bands on Pt (i.e. 2070–2080 cm^{-1}), suggesting a stronger back-donation of Pt to CO. This would decrease the bond strength and explains the observed red-shift. The origin for such effects likely stems from the highly reduced ceria surface hindering electron transfer from Pt to the ceria. This also indicates that these carbonyl species are present at the Pt-ceria interface [39–41]. Under the $^{13}CO_2/H_2$/Ar, a red-shift of this band towards 2005 cm^{-1} was observed, indicating the exchange towards ^{13}C-carbonyls on the surface of the catalyst. Similar observations were made with respect to formate species (Fig. 4b), where the Fermi resonance doublet is present for both ^{12}C and ^{13}C species, with the latter following the theoretical isotopic shift of 0.977 [42,43]. The second ν(CO), generally including bands corresponding to vibrational (C-O) stretching (1590–1510 cm^{-1}), and bending modes of formates (1390–1350 cm^{-1}) complicated discerning the nature of the bands [27,31,44]. Therefore, the last spectra of the $^{13}CO_2$-stream cycle was used as an internal background, aiding the investigation of variations between the two streams. This renders any ^{13}C-based surface species to have a negative-going band. Such analysis provided two bands at 1251 and 1605 cm^{-1}. Lopez et al. carried out the same procedure under a CuO/CeO_2 catalyst and obtained two similar bands, which they ascribed to mono or poly-dentate carbonates adsorbed on ceria [27]. Our multivariate spectral analysis using multivariate curve resolution (MCR) provided similar results, suggesting the presence of bidentate carbonate species on the support (Figure S6) [45].

The power of SSITKA-DRIFTS lies within investigating the temporal evolution of surface intermediates upon the isotopic switch, which

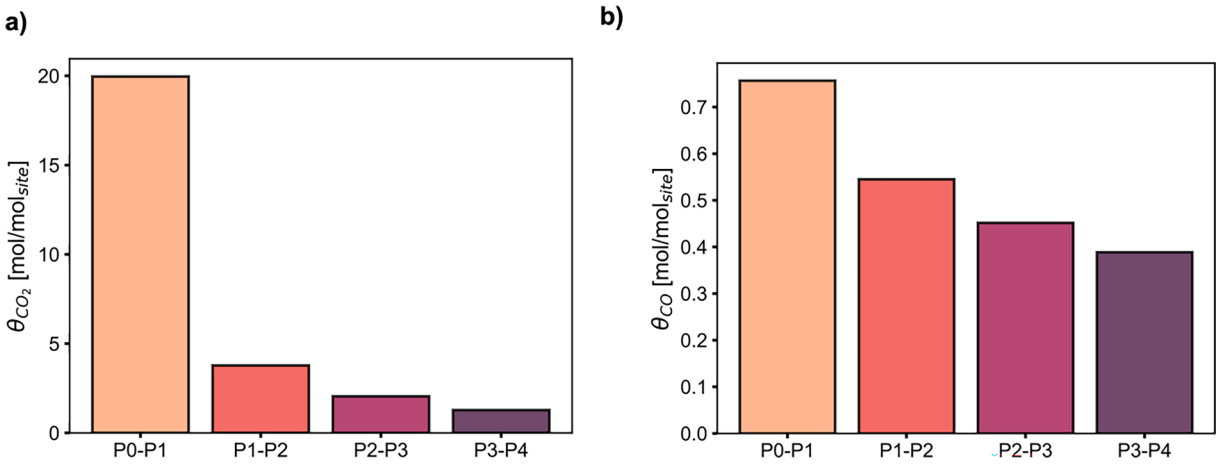

Fig. 3. Coverage of a) CO_2 and b) CO surface species on Pt calculated by means of SSITKA experiments at different positions. Conditions: $H_2/^xCO_2 = 4$ ($c_{xCO2} = 2.25$ vol%), P = 1 bar, W_{cat} = 180 mg, F = 50 NmL/min, T = 200 °C.

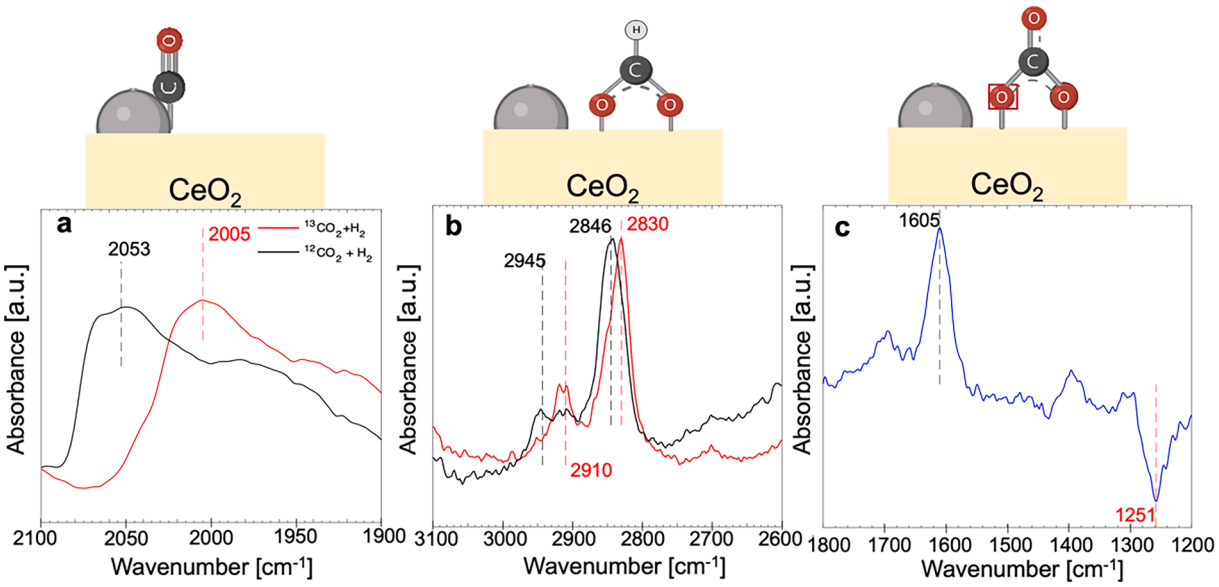

Fig. 4. Spectra under $^{12}CO_2 + H_2$ or $^{13}CO_2 + H_2$ at 200 °C. a) ν(C-O) region, b) ν(C–H) region, c) ν(CO) region. Both a and b are shown with an external background under He, whilst for c) an internal background was used (last spectra of $^{13}CO_2$ cycle) in order to allow the reader to visualize the exchange better. Red lines indicate ^{13}C-containing species, while black lines correspond to ^{12}C-containing species. Conditions: $H_2/^xCO_2 = 4$ ($c_{xCO2} = 2.25$ vol%), P = 1 bar, $W_{cat} = 180$ mg, F = 50 NmL/min.

accelerates the identification of the main surface components. For such intermediates, their exchange occurs either earlier or at a similar pace than the gas-phase product, whilst species involved to a lesser extent will experience significantly slower exchange rates compared to CO. Fig. 5 shows the surface species responses attained through MCR at different positions together with the normalized response of gaseous CO. These results readily make apparent the slower exchange of formate species, which had a surface lifetime much greater than that of CO(g) at all the positions investigated. The mechanism of the RWGS reaction has been shown to depend on the nature of the catalyst and the operating conditions [32,33,37]. In addition, the presupposed active sites have been portrayed to be highly dynamic under reaction conditions [37]. For noble-metal nanoparticles supported on reducible metal oxides, two main pathways have been proposed: a regenerative mechanism and the associative or formate pathway [21]. In the former, hydrogen species are not directly involved in the production of CO(g), and their role is limited to replenish the oxygen vacancies, which are the sites in which CO_2 reduction occurs. In the associative mechanism, the dissociated hydrogen atoms on the metal react with surface intermediates leading to formates, with the subsequent decomposition of such intermediates to CO(g) [46,47]. Considering the slow exchange of formate species, our results suggest that the associate/formate route is not the prevailing mechanism under the conditions of this study. However, at 250 °C the exchange rate of formates are drastically accelerated, possibly suggesting that this route can be favoured and possibly dominant at even higher temperatures (Figure S7). It is worth mentioning that formates are reported to lead to the formation of CO(g), albeit at lower amounts [31]. This is in line with the results reported by Goguet et al. who quantified formate species on ceria via calibration with formate impregnated on the metal oxide and stipulated that these precursors could not account for the production of CO(g) completely [20].

On the other hand, carbonate species always exchanged at a faster rate than CO(g), confirming their direct contribution. Moreover, CO_2 intermediates present in larger amounts than Pt atoms available for reaction (*vide supra*) suggests that CO_2 activation proceeds via adsorption on the ceria surface. This is seconded by both acid-base

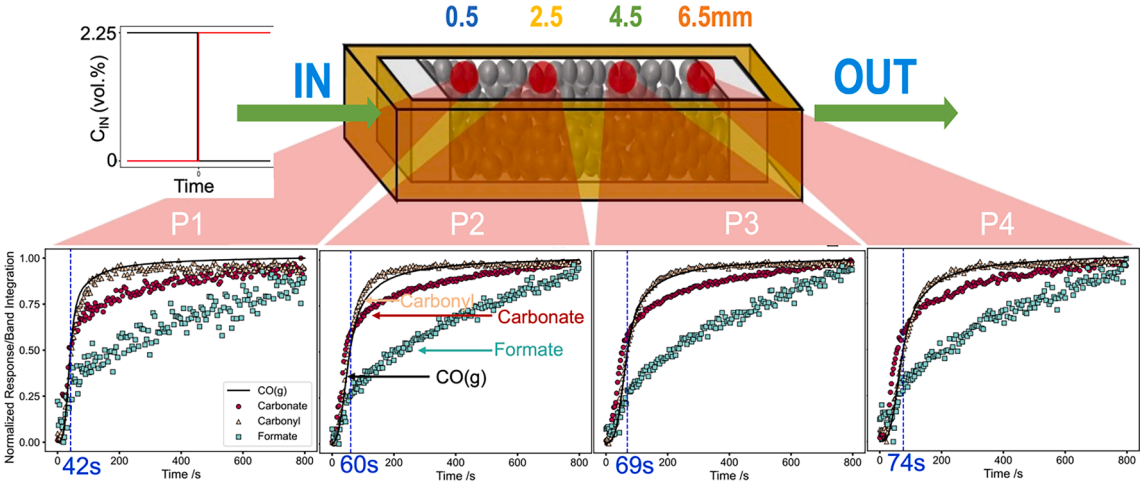

Fig. 5. Normalized surface species (scatter) and gas species (solid line) step responses after a switch from 2.25 vol% $^{12}CO_2$/9% H_2 →2.25 vol% $^{13}CO_2$/9% H_2/2.5 % Ar at 200 °C over a 3 wt% Pt/CeO_2 catalyst. Conditions: F = 50 mL/min, P = 1 bar, $W_{cat} = 180$ mg.

considerations and the well-known oxygen vacancy assisted adsorption of CO_2 [48–50], which is expected to yield bidentate carbonates. This matches with the kinetically pure spectra attained by deconvolution through MCR. The exchange rate of carbonyls markedly resembled that of gaseous CO(g) at all positions, which could be explained by either carbonyls being an intermediate or a product of the subsequent adsorption of CO(g) in proximity to the Pt-ceria interface.

In order to further investigate the role of carbonyls, the integrated absorbance of the carbonyl bands at different positions was used as an approximate indicator of the concentration of such species, shown in Fig. 6. Although DRIFT spectra do not show a direct linear relationship with concentration (i.e. Beer-Lambert law) due to the measurements being obtained in reflectance mode (although this is absorbance/system dependent [51]), the fact that the spectra at different positions were normalized to the same intensity allows us to assume that higher absorbances are directly correlated to higher concentrations of said species. As can be seen by the results, the first position displays the highest absorbance of carbonyl species, pointing to their roles as intermediates. If carbonyls would not precede the formation of CO(g), their surface concentration would have been higher at the outlet-most position, as these species would stem from the adsorption of CO(g).

3.5. Mechanistic discussion

Correlating the gaseous and surface normalized responses by means of spatially resolved gas sampling and DRIFTS, respectively, during SSITKA experiments with Pt/CeO_2 provided clear indications on the involvement of different surface intermediates. As previously described, the consensus in literature suggests the presence of a redox and associative/formate mechanisms, with oxygen vacancies having been postulated to enhance CO_2 activation and conversion [21]. In fact, many reports point to a reversal in the role of the metal and the support, where the latter actually constitutes the active sites. Our results point to this being the case for CO_2 activation, which likely occurs on ceria rather than CO_2 dissociating on Pt nanoparticles, which has also been shown to be energetically unfavorable with DFT calculations due to the low oxophilicity of Pt [33]. For materials such as CeO_2 and TiO_2, the inherent presence of oxygen vacancies under net reducing atmospheres and temperatures above 180 °C most likely assisted the activation of CO_2, yielding carbonate species [50,52]. In fact, previous research in our group pointed to oxygen vacancies being the activity descriptor within Au/TiO_2 catalysts by means of *operando* UV–Vis spectroscopy [21]. Therefore, Pt would not be directly involved in the adsorption of CO_2. However, noble-metals are known for increasing the reducibility of such metal oxides by means of electron transfer. In addition, other factors such as hydrogen spillover would also enhance the presence of oxygen vacancies, or reverse (oxygen) spillover from the support to the metal [53–56]. All these phenomena are intrinsically localized near the Pt sites. Therefore, the active carbonates formed on ceria likely lie near Pt, suggesting an important interplay between Pt and ceria. Concerning the minor roles of formates at the temperatures screened herein, at values above 300 °C, the RWGS reaction over Pt/CeO_2 has been shown to proceed through both the redox and formate pathway concurrently, leading to increased activity of these catalysts with respect to Pt/TiO_2, which are generally more active than ceria-supported catalysts at low temperature [32]. This is supported by our SSITKA-DRIFTS results, in which formates show the highest dependency on temperature out of all surface species. These temperature dependent variations further contribute to the lack of any definitive proof for catalytic pathways within RWGS catalysis.

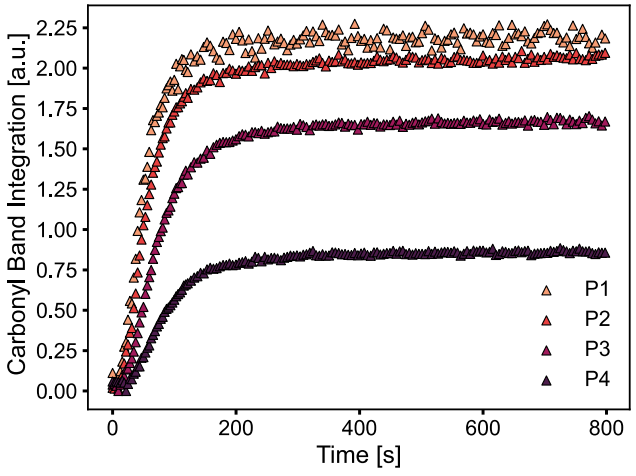

Fig. 6. Carbonyl band area at different positions over time after a switch from 2.25 vol% $^{12}CO_2$/9% H_2 →2.25 vol% $^{13}CO_2$/9% H_2/2.5 % Ar at 200 °C. Conditions: F = 50 mL/min, P = 1 bar, W_{cat} = 180 mg.

The pathway for the subsequent decomposition of carbonates still remains unclear within the literature, although insights seem to point at two different possibilities: direct carbonate decomposition or carbonate decomposition via a Pt-bound carbonyl, as shown in Scheme 1. In the former, the production of CO(g) would re-oxidize the ceria surface without any participation of Pt atoms. On the other hand, the latter route suggests that Pt aids in the decomposition of carbonates either by charge transfer and/or providing a vicinal site for the subsequent adsorption of CO. Having previously established the presence of these carbonyls at the Pt-ceria interface and the close proximity of carbonate species to Pt, both routes seem possible. This possibility has been widely discussed within the literature, with Goguet et al. first proposing these two routes [11,20]. Herein, we show that spatial resolution provides further insights into the role of carbonyls. As previously described, the coverage of carbonyls was found to be largest at the inlet position of the bed, which strongly put forward their involvement as intermediates. This is due to the concentration of intermediates stemming directly from that of the reactants, which is inherently higher at the inlet of the reactor. If carbonyls would have been a result of the adsorption of CO(g) onto Pt, our results would have portrayed a larger coverage of these species at the outlet, where CO(g) concentration is largest. Therefore, it is likely that over Pt/CeO_2 the reaction proceeds via a special redox pathway, in which the Pt is in fact directly involved in the production of CO(g). Consequently, Pt does not simply act as a site for hydrogen activation, but also its interface with the ceria surface could also catalyze the formation of CO(g). This could also explain why activity of Pt/CeO_2 catalysts is largely dependent on the length of the Pt-CeO_2 interface [57,58]. Over WGS conditions, Kalamaras et al. reported ceria-supported Pt catalysts to undergo a similar mechanism [32].

This mechanism is substantially different from the proposed route for the RWGS reaction over Au nanoparticles supported on reducible metal oxides, in which the main intermediate is believed to be a hydroxylcarbonyl (OCOH), stemming from the interaction of inbound CO_2 and H within the Au surface [59]. In addition, carbonates species on Au/TiO_2 are believed to be spectator species, which is not the case for Pt/CeO_2.

3.6. Kinetic modeling

The capabilities of the spatially-resolved SSITKA with the aim to enhance the determination of kinetic parameters were also tested. This should also aid in the determination of the most plausible reaction mechanism. As in all kinetic models, the governing equations of the reactor system at hand are solved through considering different sets of reactions, aiming at finding which kinetic model describes the experimental data more accurately. In our case, all spatially resolved profiles were used as input simultaneously, aiming at enhancing the decoupling of kinetics and transport phenomena. Importance should be given to using all experimental data concurrently for optimization, to ensure that the same kinetic parameters are obtained throughout the reactor.

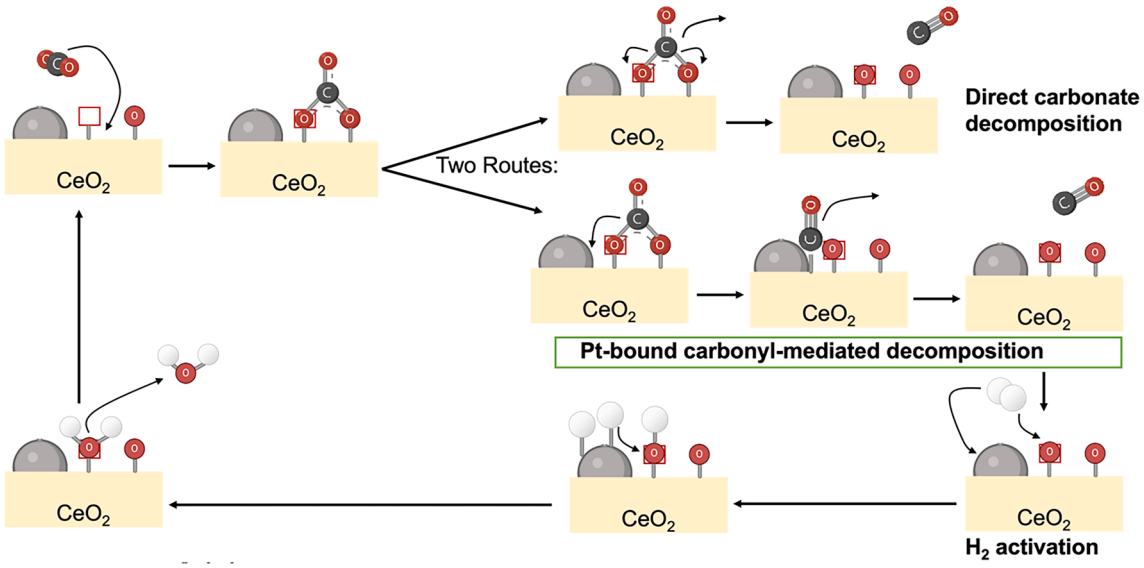

Scheme 1. Representation of the regenerative/redox mechanism for the RWGS reaction over Pt/CeO_2 at low temperatures.

Moreover, the previously described two plausible mechanisms involving the direct decomposition of carbonates and the pathway involving carbonyls at the Pt-ceria interface were considered in the form of their respective elementary reaction steps. No assumptions such as quasi steady-state assumption (QSSA) or reaction equilibrium assumption (REA) were applied due to spatial resolution providing enough data points for all of the kinetic parameters to be fitted.

The results for both models are presented in Fig. 7. It shows that when the involvement of Pt in such decomposition was included within the elementary reaction steps, the agreement with the experimental data was much more accurate. These computations further indicate that the RDS corresponds to either the water formation or the diffusion of hydrogen towards the oxidized ceria surface (see Table S3). This is in agreement with our SSITKA results, indicating that the RDS does not involve the participation of any C-containing species. In addition, these findings also suggest the importance of oxygen vacancies and surface hydroxyls, with their regeneration being the rate limiting step. These results imply that further improvement of Pt/CeO_2 could be achieved through facilitating the spillover of hydrogen and the subsequent regeneration of oxygen vacancies.

4. Conclusions

This work set out to demonstrate how the application of concepts generally only considered in chemical engineering (i.e. continuity equation considerations) could be helpful at determining reaction mechanisms. The coupling of SSITKA with spatiotemporally resolved methodologies such as MS gas sampling and *operando* DRIFTS during RWGS conditions over Pt/CeO_2, allowed to gain insight into the reaction mechanism. Comparison between the exchange rates of surface species and gaseous CO readily showed the important role of reducible oxides in RWGS catalysis, with the oxygen vacancies likely being directly involved in the reaction mechanism by means of CO_2 activation in the form of carbonates. In addition, the possible participation of formates as intermediate was ruled out, although their participation becomes increasingly important at higher temperatures.

Moreover, specifically thanks to spatial resolution, we determine the participation of carbonyls as intermediates, which has been debated for decades, suggesting that spatial resolution could aid the investigation of the role of surface species. The direct participation of carbonyls at the metal-support interface further indicates the importance of the interplay between Pt and ceria.

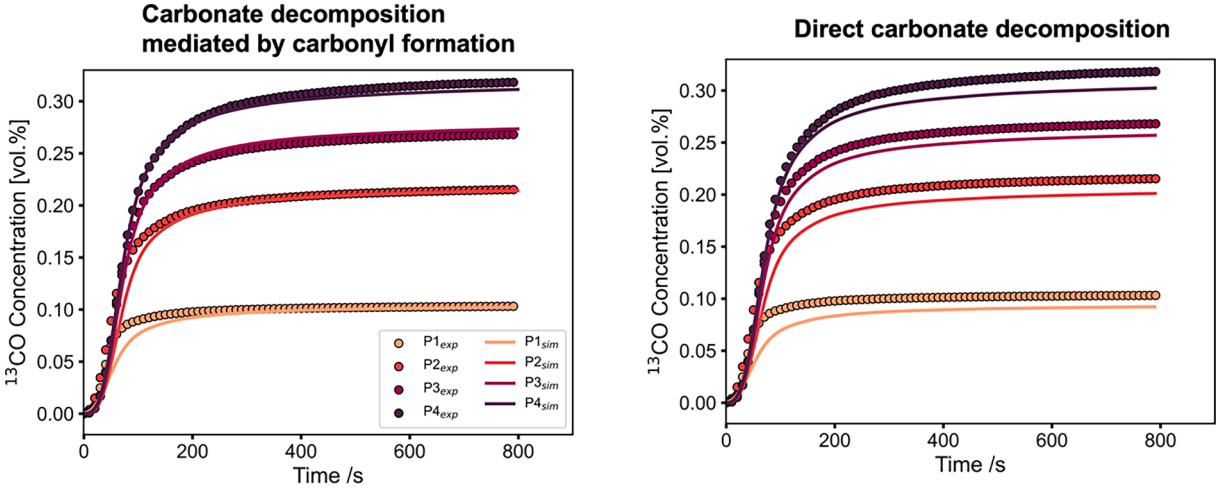

Fig. 7. Kinetic modelling results for the two proposed sets of elementary reactions, showing the experimental (scatter) and simulated (solid line) data. Conditions: F = 50 mL/min, P = 1 bar, W_{cat} = 180 mg, T = 200 °C.

Altogether, it is believed that this methodology could provide deepened insights into the kinetics governing steady state reactions, and the coupling of multimodal experimental and computational techniques constitutes an attractive route towards more complete insight into the system at hand, allowing to observe the catalysts under true working conditions.

CRediT authorship contribution statement

Damián Vico van Berkel: Conceptualization, Methodology, Software, Validation, Investigation, Formal analysis, Writing – original draft, Visualization. **Atsushi Urakawa:** Conceptualization, Methodology, Supervision, Writing – review & editing.

Declaration of competing interest

The authors declare that they have no known competing financial interests or personal relationships that could have appeared to influence the work reported in this paper.

Data availability

Data will be made available on request.

Appendix A. Supplementary material

Supplementary material to this article can be found online at https://doi.org/10.1016/j.jcat.2024.115470.

References

[1] A. Bruix, J.T. Margraf, M. Andersen, K. Reuter, First-principles-based multiscale modelling of heterogeneous catalysis, Nat. Cataly. 282 (2019) 659–670, https://doi.org/10.1038/s41929-019-0298-3.

[2] R.J. Berger, F. Kapteijn, J.A. Moulijn, G.B. Marin, J. De Wilde, M. Olea, D. Chen, A. Holmen, L. Lietti, E. Tronconi, Y. Schuurman, Dynamic methods for catalytic kinetics, Appl. Catal. A Gen 342 (2008) 3–28, https://doi.org/10.1016/j.apcata.2008.03.020.

[3] R.J. Berger, J. Pérez-Ramírez, F. Kapteijn, J.A. Moulijn, Catalyst performance testing: the influence of catalyst bed dilution on the conversion observed, Chem Eng J 90 (2002) 173–183, https://doi.org/10.1016/S1385-8947(02)00078-5.

[4] C. Ledesma, J. Yang, D. Chen, A. Holmen, Recent approaches in mechanistic and kinetic studies of catalytic reactions using SSITKA technique, ACS Catal. 4 (2014) 4527–4547, https://doi.org/10.1021/cs501264f.

[5] A. Urakawa, Mind the gaps in CO_2-to-methanol, Nat. Catal. 4 (2021) 447–448, https://doi.org/10.1038/s41929-021-00638-6.

[6] A. Urakawa, T. Bürgi, A. Baiker, Sensitivity enhancement and dynamic behavior analysis by modulation excitation spectroscopy: principle and application in heterogeneous catalysis, Chem. Eng. Sci. 63 (2008) 4902–4909, https://doi.org/10.1016/j.ces.2007.06.009.

[7] X. Wang, H. Shi, J. Szanyi, Controlling selectivities in CO_2 reduction through mechanistic understanding, Nat. Commun. 8 (2017) 1–6, https://doi.org/10.1038/s41467-017-00558-9.

[8] P. Biloen, Transient kinetic methods, J. Mol. Catal. 21 (1983) 17–24, https://doi.org/10.1016/0304-5102(93)80108-7.

[9] Y. Soong, K. Krishna, P. Biloen, Catalyst aging studied with isotopic transients: methanation over raney nickel, J. Catal. 97 (1986) 330–343, https://doi.org/10.1016/0021-9517(86)90005-9.

[10] P. Biloen, J.N. Helle, F.G.A. van den Berg, W.M.H. Sachtler, On the activity of fischer-tropsch and methanation catalysts: a study utilizing isotopic transients, J. Catal. 81 (1983) 450–463, https://doi.org/10.1016/0021-9517(83)90183-5.

[11] F.C. Meunier, D. Tibiletti, A. Goguet, D. Reid, R. Burch, On the reactivity of carbonate species on a Pt/CeO_2 catalyst under various reaction atmospheres: application of the isotopic exchange technique, Appl. Catal. A 289 (2005) 104–112, https://doi.org/10.1016/j.apcata.2005.04.018.

[12] M.A. Vasiliades, K.K. Kyprianou, N.S. Govender, A. Govender, R. Crous, D. Moodley, A.M. Efstathiou, The effect of CO Partial pressure on important kinetic parameters of methanation reaction on co-based FTS catalyst studied by SSITKA-MS and operando DRIFTS-MS techniques, Catalysts 10 (2020) 583, https://doi.org/10.3390/catal10050583.

[13] D. Tibiletti, A. Goguet, D. Reid, F.C. Meunier, R. Burch, On the need to use steady-state or operando techniques to investigate reaction mechanisms: an in situ DRIFTS and SSITKA-based study example, Catal. Today 113 (2006) 94–101, https://doi.org/10.1016/j.cattod.2005.11.013.

[14] M.A. Vasiliades, N.S. Govender, A. Govender, R. Crous, D. Moodley, T. Botha, A. M. Efstathiou, The effect of H_2 pressure on the Carbon path of methanation reaction on Co/γ-Al_2O_3: transient isotopic and operando methodology studies, ACS Catal. 12 (2022) 15110–15129, https://doi.org/10.1021/ACSCATAL.2C04269.

[15] A.M. Gä, M. Casapu, D.E. Doronkin, F. Maurer, P. Lott, P. Glatzel, M. Votsmeier, O. Deutschmann, J.-D. Grunwaldt, Unravelling the different reaction pathways for low temperature CO oxidation on Pt/CeO_2 and Pt/Al_2O_3 by spatially resolved structure−activity correlations, J. Phys. Chem. Lett. 10 (2019) 7698–7705, https://doi.org/10.1021/acs.jpclett.9b02768.

[16] D. Pinto, V. van der Bom Estadella, A. Urakawa, Mechanistic insights into the CO_2 capture and reduction on K-promoted Cu/Al_2O_3 by spatiotemporal operando methodologies, Catal. Sci Technol 12 (2022) 5349–5359, https://doi.org/10.1039/D2CY00228K.

[17] K. Morgan, J. Touitou, J.S. Choi, C. Coney, C. Hardacre, J.A. Pihl, C.E. Stere, M. Y. Kim, C. Stewart, A. Goguet, W.P. Partridge, Evolution and enabling capabilities of spatially resolved techniques for the characterization of heterogeneously catalyzed reactions, ACS Catal. 6 (2016) 1356–1381, https://doi.org/10.1021/acscatal.5b02602.

[18] L. van Beek, D. Jain, P. Gholkar, T.J. Eldridge, H.P. Nguyen, K. Muramoto, A. Urakawa, Spatiotemporal operando UV-vis spectroscopy: development and mechanistic alternation of CO oxidation on Pt/Al_2O_3 on the reactor scale, Catal. Today 429 (2024) 114466, https://doi.org/10.1016/j.cattod.2023.114466.

[19] A. Urakawa, N. Maeda, A. Baiker, A. Urakawa, N. Maeda, A. Baiker, Space- and time-resolved combined DRIFT and raman spectroscopy: monitoring dynamic surface and bulk processes during NOx storage reduction, Angew. Chem. Int. Ed. 47 (2008) 9256–9259, https://doi.org/10.1002/anie.200804077.

[20] A. Goguet, F.C. Meunier, D. Tibiletti, J.P. Breen, R. Burch, Spectrokinetic investigation of reverse water-gas-shift reaction intermediates over a Pt/CeO_2 catalyst, J. Phys. Chem. B 108 (52) (2004) 20240–20246, https://doi.org/10.1021/jp047242w.

[21] L.F. Bobadilla, J.J. Santos, S. Ivanova, J.J. Odriozola, A. Urakawa, Unravelling the role of oxygen vacancies in the mechanism of the reverse water−gas shift reaction by operando DRIFTS and ultraviolet−visible spectroscopy, ACS Catal. 8 (2018) 7455–7467, https://doi.org/10.1021/acscatal.8b02121.

[22] A. Goguet, F. Meunier, J.P. Breen, R. Burch, M.I. Petch, A. Faur Ghenciu, Study of the origin of the deactivation of a Pt/CeO2 catalyst during reverse water gas shift (RWGS) reaction, J. Catal. 226 (2004) 382–392, https://doi.org/10.1016/j.jcat.2004.06.011.

[23] A. Goguet, S.O. Shekhtman, R. Burch, C. Hardacre, F.C. Meunier, G.S. Yablonsky, Pulse-response TAP studies of the reverse water–gas shift reaction over a Pt/CeO_2 catalyst, J. Catal. 237 (2006) 102–110, https://doi.org/10.1016/j.jcat.2005.10.020.

[24] S.L. Shannon, J.G. Goodwin, Characterization of catalytic Surfaces by isotopic-transient kinetics during steady-state reaction, Chem. Rev. 95 (1995) 677–695, https://doi.org/10.1021/cr00035a011.

[25] M. Gómez-Gallego, M.A. Sierra, Kinetic isotope effects in the study of organometallic reaction mechanisms, Chem. Rev. 111 (2011) 4857–4963, https://doi.org/10.1021/cr100436k.

[26] C.M. Kalamaras, G.G. Olympiou, A.M. Efstathiou, The water-gas shift reaction on Pt/γ-Al_2O_3 catalyst: operando SSITKA-DRIFTS-mass spectroscopy studies, Catal. Today 138 (2008) 228–234, https://doi.org/10.1016/j.cattod.2008.06.010.

[27] A.L. Cámara, S. Chansai, C. Hardacre, A. Martínez-Arias, The water-gas shift reaction over CeO_2/CuO: operando SSITKA-DRIFTS-mass spectrometry study of low temperature mechanism, Int. J. Hydrogen Energy 39 (2014) 4095–4101, https://doi.org/10.1016/j.ijhydene.2013.05.087.

[28] D. Liu, Y. Li, M. Kottwitz, B. Yan, S. Yao, A. Gamalski, D. Grolimund, O. V. Safonova, M. Nachtegaal, J.G. Chen, E.A. Stach, R.G. Nuzzo, A.I. Frenkel, Identifying dynamic structural changes of active sites in Pt-Ni bimetallic catalysts using multimodal approaches, ACS Catal. 8 (2018) 4120–4131, https://doi.org/10.1021/acscatal.8b00706.

[29] S.H. Ali, J.G. Goodwin, Impact of readsorption effects and their removal from surface reaction parameters obtained by isotopic transient kinetic analysis: methanol synthesis on Pd/SiO_2, J. Catal. 171 (1997) 339–344, https://doi.org/10.1006/jcat.1997.1778.

[30] F.C. Meunier, D. Tibiletti, A. Goguet, S. Shekhtman, C. Hardacre, R. Burch, On the complexity of the water-gas shift reaction mechanism over a Pt/CeO_2 catalyst: effect of the temperature on the reactivity of formate surface species studied by operando DRIFT during isotopic transient at chemical steady-state, Catal. Today 126 (2007) 143–147, https://doi.org/10.1016/j.cattod.2006.10.003.

[31] F.C. Meunier, D. Reid, A. Goguet, S. Shekhtman, C. Hardacre, R. Burch, W. Deng, M. Flytzani-Stephanopoulos, Quantitative analysis of the reactivity of formate species seen by DRIFTS over a Au/Ce(La)O_2 water–gas shift catalyst: first unambiguous evidence of the minority role of formates as reaction intermediates, J. Catal. 247 (2007) 277–287, https://doi.org/10.1016/j.jcat.2007.02.013.

[32] C.M. Kalamaras, I.D. Gonzalez, R.M. Navarro, J.L.G. Fierro, A.M. Efstathiou, Effects of reaction temperature and support composition on the mechanism of water - gas shift reaction over supported-Pt catalysts, J. Phys. Chem. C 115 (2011) 11595–11610, https://doi.org/10.1021/jp201773a.

[33] L. Dietz, S. Piccinin, M. Maestri, Mechanistic insights into CO_2 activation via reverse water−gas shift on metal surfaces, (2015), J. Phys. Chem. C 119 (9) (2015) 4959–4966, https://doi.org/10.1021/jp512962c.

[34] A. Chen, X. Yu, Y. Zhou, S. Miao, Y. Li, S. Kuld, J. Sehested, J. Liu, T. Aoki, S. Hong, M.F. Camellone, S. Fabris, J. Ning, C. Jin, C. Yang, A. Nefedov, C. Wöll, Y. Wang, W. Shen, Structure of the catalytically active copper–ceria interfacial perimeter, Nat. Catal. 2 (2019) 334–341, https://doi.org/10.1038/s41929-019-0226-6.

[35] M.J. Lundwall, S.M. McClure, D.W. Goodman, Probing terrace and step sites on Pt nanoparticles using Co and ethylene, J. Phys. Chem. C 114 (2010) 7904–7912, https://doi.org/10.1021/jp9119292.

[36] P. Bazin, O. Saur, J.C. Lavalley, M. Daturi, G. Blanchard, FT-IR study of CO adsorption on Pt/CeO_2: characterisation and structural rearrangement of small pt particles, Phys. Chem. Chem. Phys. 7 (2005) 187–194, https://doi.org/10.1039/b414159h.

[37] Y. Li, M. Kottwitz, J.L. Vincent, M.J. Enright, Z. Liu, L. Zhang, J. Huang, S. D. Senanayake, W.C.D. Yang, P.A. Crozier, R.G. Nuzzo, A.I. Frenkel, Dynamic structure of active sites in ceria-supported pt catalysts for the water gas shift reaction, Nat. Commun. 12 (2021) 1–9, https://doi.org/10.1038/s41467-021-21132-4.

[38] A.M. Efstathiou, Elucidation of mechanistic and kinetic aspects of water-gas shift reaction on supported Pt and Au catalysts via transient isotopic techniques, Catalysis (2016) 175–236, https://doi.org/10.1039/9781782626855-00175.

[39] Y. Lykhach, S.M. Kozlov, T. Skála, A. Tovt, V. Stetsovych, N. Tsud, F. Dvořák, V. Johánek, A. Neitzel, J. Mysliveček, S. Fabris, V. Matolín, K.M. Neyman, J. Libuda, Counting electrons on supported nanoparticles, Nat. Mater. 15 (2016) 284–288, https://doi.org/10.1038/nmat4500.

[40] A. Bruix, J.J. Rodriguez, P.J. Ramírez, S.D. Senanayake, J. Evans, J.B. Park, D. Stacchiola, P. Liu, J. Hrbek, F. Illas, A new type of strong Metal−Support Interaction and the production of H_2 through the transformation of water on pt/CeO_2 (111) and Pt/CeOx /TiO_2 (110) catalysts, J. Am. Chem. Soc. 134 (21) (2012) 8968–8974, https://doi.org/10.1021/ja302070k.

[41] J.C. Frost, Junction effect interactions in methanol synthesis catalysts, Nature 334 (6183) (1988) 577–580, https://doi.org/10.1038/334577a0.

[42] G.N. Vayssilov, M. Mihaylov, P. St Petkov, K.I. Hadjiivanov, K.M. Neyman, Reassignment of the vibrational spectra of carbonates, formates, and related surface species on ceria: a combined density functional and infrared spectroscopy investigation, J. Phys. Chem. C 115 (2011) 23435–23454, https://doi.org/10.1021/jp208050a.

[43] C. Li, Y. Sakata, T. Arai, K. Domen, K.-I. Maruya, T. Onishi, Adsorption of carbon monoxide and carbon dioxide on cerium oxide studied by fourier-transform Infrared spectroscopy Part 2. -formation of formate species on partially reduced CeO, at room temperature, J. Chem. Soc., Faraday Trans. I (85) (1989) 1451–1461.

[44] P. Bera, A.L. Cámara, A. Hornés, A. Martínez-Arias, Comparative in situ DRIFTS-MS study of ^{12}CO-and ^{13}CO-TPR on CuO/CeO_2 catalyst, J. Phys. Chem. C 113 (24) (2009) 10689–10695, https://doi.org/10.1021/jp9020504.

[45] J. Jaumot, A. de Juan, R. Tauler, MCR-ALS GUI 2.0: new features and applications, Chemom. Intell. Lab. Syst. 140 (2015) 1–12, https://doi.org/10.1016/j.chemolab.2014.10.003.

[46] R.J. Gorte, S. Zhao, Studies of the water-gas-shift reaction with ceria-supported precious metals, Catal. Today 104 (2005) 18–24, https://doi.org/10.1016/j.cattod.2005.03.034.

[47] X. Wang, R.J. Gorte, J.P. Wagner, Deactivation mechanisms for Pd/Ceria during the water–gas-shift reaction, J. Catal. 212 (2002) 225–230, https://doi.org/10.1006/jcat.2002.3789.

[48] S. Poto, D. Vico van Berkel, F. Gallucci, M.F. Neira d'Angelo, Kinetic modelling of the methanol synthesis from CO_2 and H_2 over a CuO/CeO_2/ZrO_2 catalyst: the role of CO_2 and CO hydrogenation, Chem. Eng. J. 435 (2022) 134946, https://doi.org/10.1016/J.CEJ.2022.134946.

[49] A. Parastaev, V. Muravev, E. Huertas Osta, A.J.F. van Hoof, T.F. Kimpel, N. Kosinov, E.J.M. Hensen, Boosting CO_2 hydrogenation via size-dependent metal–support interactions in cobalt/ceria-based catalysts, Nat. Catal. 3 (2020) 526–533, https://doi.org/10.1038/s41929-020-0459-4.

[50] C.T. Campbell, C.H.F. Peden, Oxygen vacancies and catalysis on ceria surfaces, Science 309 (2005) 713–714, https://doi.org/10.1126/science.1113955.

[51] J. Sirita, S. Phanichphant, F.C. Meunier, Quantitative analysis of adsorbate concentrations by diffuse reflectance FT-IR, Anal. Chem. 79 (2007) 3912–3918, https://doi.org/10.1021/ac0702802.

[52] L. Nie, D. Mei, H. Xiong, B. Peng, Z. Ren, X.I.P. Hernandez, A. DeLaRiva, M. Wang, M.H. Engelhard, L. Kovarik, A.K. Datye, Y. Wang, Activation of surface lattice oxygen in single-atom Pt/CeO_2 for low-temperature CO oxidation, Science 358 (2017) 1419–1423, https://doi.org/10.1126/science.aao2109.

[53] A. Beck, D. Kazazis, Y. Ekinci, X. Li, E.A. Müller Gubler, A. Kleibert, M.G. Willinger, L. Artiglia, J.a. Van Bokhoven, The extent of platinum-induced hydrogen spillover on cerium dioxide, ACS Nano 17 (2022) 1091–1099, https://doi.org/10.1021/acsnano.2c08152.

[54] A. Mahdavi-Shakib, T.N. Whittaker, T.Y. Yun, K.B. Sravan Kumar, L.C. Rich, S. Wang, R.M. Rioux, L.C. Grabow, B.D. Chandler, The role of surface hydroxyls in the entropy-driven adsorption and spillover of H_2 on Au/TiO_2 catalysts, Nat. Catal. 6 (2023) 710–719, https://doi.org/10.1038/s41929-023-00996-3.

[55] W. Karim, C. Spreafico, A. Kleibert, J. Gobrecht, J. Vandevondele, Y. Ekinci, J. A. Van Bokhoven, Catalyst support effects on hydrogen spillover, Nature 541 (2017) 68–71, https://doi.org/10.1038/nature20782.

[56] G.N. Vayssilov, Y. Lykhach, A. Migani, T. Staudt, G.P. Petrova, N. Tsud, T. Skála, A. Bruix, F. Illas, K.C. Prince, V. Matolín, K.M. Neyman, J. Libuda, Support nanostructure boosts oxygen transfer to catalytically active platinum nanoparticles, Nat. Mater. 10 (2011) 310–315, https://doi.org/10.1038/nmat2976.

[57] L.R. Borges, A.H. Braga, D. Zanchet, J.M.R. Gallo, J.M.C. Bueno, CeO2/Pt/Al2O3 catalysts for the WGS reaction: improving understanding of the Pt-O-Ce-Ox interface as an active site, Appl. Catal. B 325 (2023) 122361, https://doi.org/10.1016/j.apcatb.2023.122361.

[58] C.M. Kalamaras, D.D. Dionysiou, A.M. Efstathiou, Mechanistic studies of the water-gas shift reaction over Pt/$Ce_xZr_{1-x}O_2$ catalysts: the effect of Pt particle size and Zr dopant, ACS Catal. 2 (2012) 2729–2742, https://doi.org/10.1021/cs3006204.

[59] J.A. Rodriguez, P. Liu, D.J. Stacchiola, S.D. Senanayake, M.G. White, J.G. Chen, Hydrogenation of CO_2 to methanol: importance of metal-oxide and metal-Carbide Interfaces in the activation of CO_2, ACS Catal. 5 (2015) 6696–6706, https://doi.org/10.1021/acscatal.5b01755.